HHS Public Access

Author manuscript

J Tissue Eng Regen Med. Author manuscript; available in PMC 2019 June 26.

Published in final edited form as:

J Tissue Eng Regen Med. 2018 April ; 12(4): 1039–1048. doi:10.1002/term.2605.

Cell-laden composite suture threads for repairing damaged tendons

Raquel Costa-Almeida[1,2,3,4], **Rui M.A. Domingues**[1,2], **Afsoon Fallahi**[3,4,5], **Huseyin Avci**[3,4,6], **Iman K. Yazdi**[3,4,5], **Mohsen Akbari**[3,4,5], **Rui L. Reis**[1,2,7], **Ali Tamayol**[3,4,5], **Manuela E. Gomes**[1,2,7], and **Ali Khademhosseini**[3,4,5]

[1]3B's Research Group—Biomaterials, Biodegradables and Biomimetics, University of Minho, Headquarters of the European Institute of Excellence on Tissue Engineering and Regenerative Medicine, Guimarães, Portugal

[2]ICVS/3B's—PT Government Associate Laboratory, Braga, Portugal

[3]Department of Biomedical Engineering, Biomaterials Innovation Research Center, Cambridge, MA, USA

[4]Harvard-MIT Division of Health Sciences and Technologies, Massachusetts Institute of Technology, Cambridge, MA, USA

[5]Wyss Institute for Biologically Inspired Engineering, Harvard University, Cambridge, MA, USA

[6]Eskisehir Osmangazi University, Metallurgical and Materials Engineering, Eskisehir, Turkey

[7]The Discoveries Centre for Regenerative and Precision Medicine, Headquarters at University of Minho, Guimarães, Portugal

Abstract

Tendons have limited regenerative capacity due to their low cellularity and hypovascular nature, which results in poor clinical outcomes of presently used therapies. As tendon injuries are often observed in active adults, it poses an increasing socio-economic burden on healthcare systems. Currently, suture threads are used during surgical repair to anchor the tissue graft or to connect injured ends. Here, we created composite suture threads coated with a layer of cell-laden hydrogel that can be used for bridging the injured tissue aiming at tendon regeneration. In addition, the fibres can be used to engineer 3-dimensional constructs through textile processes mimicking the architecture and mechanical properties of soft tissues, including tendons and ligaments. Encapsulated human tendon-derived cells migrated within the hydrogel and aligned at the surface of the core thread. An up-regulation of tendon-related genes (scleraxis and tenascin C) and genes involved in matrix remodelling (matrix metalloproteinases 1, matrix metalloproteinases 2) was

Correspondence Ali Tamayol and Manuela E. Gomes, 3B's Research Group—Biomaterials, Biodegradables and Biomimetics, University of Minho, Headquarters of the European Institute of Excellence on Tissue Engineering and Regenerative Medicine, AvePark—Parque de Ciência eTecnologia, Zona Industrial da Gandra, 4805-017 Barco, Guimarães, Portugal. atamayol@mit.edu; megomes@dep.uminho.pt.

CONFLICT OF INTEREST

The authors have declared that there is no conflict of interest.

SUPPORTING INFORMATION

Additional Supporting Information may be found online in the supporting information tab for this article.

observed. Cells were able to produce a collagen-rich matrix, remodelling their micro-environment, which is structurally comparable to native tendon tissue.

Keywords

biotextiles; braiding; cell-laden fibres; composite sutures; tendon tissue engineering; tissue regeneration

1 | INTRODUCTION

Tendon injuries account for a considerable share of musculoskeletal disorders. In fact, over 30 million human tendon-related procedures are estimated to take place annually worldwide (Lomas et al., 2015). Besides conservative treatments, currently used therapeutic approaches to tendon injuries include surgical repair, which frequently involves the connection of the ends of injured tissue using surgical sutures, as well as application of auto- or allografts, having associated complications, including the risk of nerve injury, infection, and scarring. More importantly, the number of donors and autografts is limited and does not match the number of recipients. Tendons have a limited regenerative capacity due to their low cellular content and hypovascular nature. Thus, even surgical procedures might also fail to restore tendon function completely, which can result in permanent disability especially to patients suffering from sport-related injuries. The poor clinical outcome of presently used therapies poses an increasing socio-economic burden on healthcare systems. Thus, there is a strong need for the development of new paradigm that can facilitate the healing of damaged tendons. Tissue engineering approaches that can either facilitate the healing of the damaged tissue or can form alternative tissue substitutes hold a great promise for improving patient's quality of life. Therefore, we propose to engineer artificial yet biological tendon grafts by assembling composite fibres with encapsulated cells into three-dimensional constructs, enabling the formation of a tendon-specific micro-environment.

Fibre and textile-based technologies constitute powerful tools for engineering load bearing fibrous tissues such as tendons, ligaments, and skeletal muscles (Akbari et al., 2016; Fallahi, Khademhosseini, & Tamayol, 2016; Wang, Wu, Guo, & Ma, 2015; Wu et al., 2016; Younesi, Islam, Kishore, Anderson, & Akkus, 2014). During surgical repair of tendons, sutures are used either to anchor the tissue graft or to connect the injured ends; however, their success has been limited as these tissues have few cells to support their regeneration.

Several fabrication methods have been explored and refined over the years, including electrospinning (Domingues et al., 2016), wetspinning (Sibaja et al., 2015; Zhang et al., 2014), microfluidics (Onoe et al., 2013), and microfluidic spinning (Kang et al., 2011) to fabricate cell-laden fibres. Nonetheless, engineering functional tendons requires a multicomponent, multi-scale approach, which is far from being achieved by only one of the aforementioned techniques. Composite fibres (CFs) have been developed as a novel biofabrication tool toward fabricating multifunctional units that can be further assembled through textile techniques (Akbari et al., 2014). These core-shell CFs are comprised of a mechanically robust core and a cell-laden hydrogel shell (Akbari et al., 2014). The core fibre can provide adequate mechanical properties at the tissue-level, whereas a hydrogel shell can

replicate the hydrated biomimetic environment at the cellular-level supporting cellular growth and maturation. In this study, we developed suture threads coated with a hydrogel layer composed of alginate (ALG) and methacrylated gelatin (GelMA) for either repairing damaged tendons or engineering tendon substitutes. Herein, as an initial assessment of the biological performance of developed CFs, human tendon-derived cells (hTDCs) were encapsulated, and their behavior was evaluated.

2 | MATERIALS AND METHODS

2.1 | Materials

Non-absorbable braided surgical suturing threads (SURGISILK, DW2901R) were purchased from Sutures (Sutures Ltd., UK) and used as received. Type A gelatin from porcine skin, low viscosity sodium ALG derived from brown algae (Mw = 538 kDa, viscosity ~250 cP), calcium chloride ($CaCl_2$), methacrylic anhydride (MA, 276685), the photoinitiator 2-hydroxy-4′-(2-hydroxyethoxy)-2-methylpropiophenone 98% (Irgacure 2959) and phosphate buffered saline (PBS) were purchased from Sigma-Aldrich. Hank's Balanced Salt Solution (HBSS, with calcium and magnesium, no phenol red), Minimum Essential Medium alpha (α-MEM), fetal bovine serum (FBS), and an antibiotic/antimycotic solution (AB/AM) were purchased from Life Technologies. A final α-MEM solution was prepared with 10% (*v*/*v*) FBS and 1% AB/AM (*v*/*v*).

Sodium ALG was dissolved in PBS at a desired concentration and freshly used after preparation. Gelatin was further modified as described elsewhere (Akbari et al., 2014) to obtain GelMA.

2.2 | Cell culture

hTDCs were isolated from human tendon tissue samples collected under an established protocol with Hospital da Prelada (Porto, Portugal), as described elsewhere (Costa-Almeida et al., 2016). All samples were obtained under informed consent, according to the Declaration of Helsinki, and the protocols were approved by the ethical committee of the hospital. hTDCs were expanded in α-MEM supplemented with 10% (*v*/*v*) FBS and 1% AB/AM (*v*/*v*) and used in Passage 3.

2.3 | Preparation of cell suspension in ALG:GelMA mixture

Cells were cultured until 80% confluency and then trypsinized. After that, 2.5×10^6 cells were suspended in 10 μl of culture medium and homogenized in 1 ml of prepolymer mixture containing 1.5% (*w*/*v*) of ALG and 10% (*w*/*v*) of GelMA (ALG:GelMA).

2.4 | Fabrication of composite fibres

Suture threads were coated with a hydrogel layer composed of ALG: GelMA, following a procedure described elsewhere (Akbari et al., 2014). ALG cross-linking occurred by immersing the coated thread in a $CaCl_2$ for 2 min, and then, GelMA was photopolymerized by exposure to ultraviolet light (320–500 nm, 1.2 mW/cm^2, EXFO OmniCure S2000) for 30 s. Hydrogel loaded with fluorescent beads was used to coat threads and inspect hydrogel

stability after braiding. Hydrogel loaded with a cell suspension was used to coat threads for biological studies.

2.5 | Mechanical tests

Instron 5542 mechanical tester (Norwood, MA, USA) with a 1 kN load cell was used to perform the mechanical tests. Three different braiding patterns were used in this study: 1 × 1 biaxial, 2 × 2 biaxial, and 1 × 1 triaxial, and the mechanical properties were compared with non-braided parallel fibres (as control) by uniaxial tensile tests. For these samples, 2 cm long fibres were held tightly between two grips of the device. The initial strain rate was set as 2.5% of the original test regional length, and the samples were stretched at a constant rate of 1 mm/min. The elastic modulus of the fibres was determined from the tangent slope of the linear section of the stress–strain curve.

2.6 | Biological studies

2.6.1 | Cell viability by live/dead assay—The viability of encapsulated cells was evaluated after 1,7, and 21 days in culture by fluorescence labelling using a live/dead assay. For this purpose, 1-cm-length CF sections were removed from culture medium and washed with sterile HBSS. Subsequently, all samples were incubated with 1 mg/mL calcein acetoxymethyl (Invitrogen, 1:500) and 1.5 mM propidium iodide (PI, Invitrogen, 1:1000) solution in HBSS for 15 min at 37 °C and washed with sterile HBSS. The same protocol was applied to 3-cm braided constructs after 1 and 21 days in culture. After that, fibre sections were visualized either under a fluorescence microscope (Imager Z1m, Zeiss) or a confocal laser scanning microscope (Leica TCS SP8, Microsystems, Wetzlar, Germany).

2.6.2 | Determination of metabolic activity by Alamar Blue assay—The metabolic activity of encapsulated cells was evaluated after up to 14 days in culture by Alamar Blue assay, according to the manufacturer's instructions (AbD SeroTec, Bio-Rad). Briefly, after each incubation time, culture medium was removed; samples were washed with sterile HBSS and incubated in 10% (*v*/*v*) Alamar Blue solution in culture medium at 37 °C, 5% CO_2 for 5 hr. The fluorescence of the supernatant was measured using a plate reader (Synergy HT, Bio-Tek Instruments, 560 nm of excitation and 590 nm of emission). Afterwards, samples were washed twice with sterile HBSS, and fresh culture medium was added. Data for each individual CF were normalized to Day 1. Cell-free fibres were used as controls.

2.6.3 | RNA isolation, reverse transcription and real-time polymerase chain reaction (RT-PCR)—After 7 and 21 days in culture, total mRNA was extracted using TRI Reagent® RNA Isolation Reagent (Sigma-Aldrich), according to the manufacturer's instructions. Then, RNA was quantified on a Nanodrop® ND-1000 spectrophotometer (ThermoFisher Scientific), and cDNA was synthesized from 50 ng of mRNA using qScript™ cDNA Synthesis Kit (Quanta BioSciences). Real-time polymerase chain reaction (RT-PCR) was performed using PerfeCTA® SYBR Green FastMix (Quanta BioSciences), following manufacturer's instructions, on RT-PCR Mastercycler ep realplex gradient S machine (Realplex, Eppendorf). Primer sequences (Eurofins Genomics, UK) were designed using Primer-BLAST tool (Table S1). Relative gene expression was quantified using Livak's

method ($2^{-\Delta\Delta Ct}$) (Livak & Schmittgen, 2001; Schmittgen & Livak, 2008). For this purpose, transcript expression of target genes was first normalized to the expression of the reference housekeeping gene glyceraldehyde-3-phosphate dehydrogenase and then to the calibrator sample (hTDCs control at Day 0). Three independent assays were performed with a minimum of four samples of each condition, and results are represented as fold change.

2.6.4 | Characterization of ECM production by immunocytochemistry—To assess the ability of encapsulated cells to produce tendon-related extracellular matrix (ECM) components, cell-laden fibres were processed for immunofluorescence analysis. After specific culturing time points, samples were fixed in 3.7% (*w*/*v*, in HBSS) of paraformaldehyde for 20 min at room temperature and permeabilized using a 0.2% (*v*/*v*, in HBSS) Triton X-100 (Sigma) solution. The blocking step was performed using 1% (*v*/*v*) of bovine serum albumin (Sigma) in HBSS, and all anti-bodies were diluted in the blocking solution. The following primary antibodies were used: Rabbit polyclonal anti-human collagen I (abcam, ab292, dilution 1:500) and rabbit polyclonal anti-human collagen III (abcam, ab7778, dilution 1:100). Cells were incubated with the primary antibodies for 1 hr at room temperature, being then washed in HBSS and subsequently incubated with the secondary antibody Alexafluor 488 donkey anti-rabbit (Life Technologies, A21206, dilution 1:1000) for 1 hr at room temperature. After, samples were rinsed in HBSS; F-actin filaments of the cytoskeleton were stained with phalloidin (Phalloidin-Tetramethylrhodamine B isothiocyanate from Amanita phalloides, P1951, Sigma, 1:200 in PBS) for 20 min; and nuclei were counterstained with 4,6—Diamidino-2-phenyindole dilactate (5 μg/μl, D9564, Sigma) for 10 min. Negative controls were performed in the absence of the primary antibody. All samples were visualized using a confocal laser scanning microscope (Leica TCS SP8, Microsystems, Wetzlar, Germany).

2.6.5 | Characterization of CFs by SEM—After culturing cell-laden constructs for specific time points, cells were fixed with 3.7% (*w*/*v*, in HBSS) of paraformaldehyde for 30 min at room temperature. Then, samples were dehydrated in a series of increasing concentrations of ethanol (20%, 30%, 50%, 80%, 90%, and 95% *v*/*v* in HBSS), being incubated in 100% ethanol overnight, and being dried using a critical point dryer (Autosamdri-815, Tousimis) for 1 hr to eliminate ethanol excess. Cross sections of the fibres without cells were obtained by cutting the samples while immersed in liquid nitrogen. Fibres were carefully mounted on sample holders using double-sided carbon adhesive tape and further gold sputtered, being then analyzed using a scanning electron microscope (SEM; JSM-6010LV, JEOL, Japan). All observations and image acquisitions were made at an acceleration voltage of 15 kV.

Additionally, the microstructure of native bovine Achilles tendon was evaluated to allow the comparison with CFs. For this, samples were first fixed in 10% (*v*/*v*) neutral buffered formalin for 1 hr and, then, dehydrated as described above. Tendon samples were mounted on aluminum stubs and sputter coated with platinum prior to morphological observation by high-resolution field scanning electron microscopy (4585, Auriga Compact, Zeiss) at an accelerating voltage of 5 kV.

2.6.6 | 2D-FFT—Matrix alignment on CFs cultured for 1 and 21 days was determined through two-dimensional fast Fourier transform (2D-FFT) as previously described (Ayres et al., 2008). SEM images were first converted to 8-bit grayscale and cropped 1002–1002 pixels for 2D-FFT analysis with Image J software (NIH, USA), supported by oval profile plug-in (http://rsbweb.nih.gov/ij/plugins/oval-profile.html). The radial intensities of the 2D-FFT frequency plots were calculated and plotted against the angle of rotation from 0° to 360°. To compare directly the samples, the exported values of intensity were normalized and plotted in arbitrary units.

2.7 | Statistical analyses

Results are presented as mean ± standard error of the mean. Statistical analyses were performed using GaphPad Prism 6.0 software. One-way analysis of variance with post-hoc Tukey tests was performed. A difference between experimental groups was considered significant with a confidence interval of 95%, whenever $p < 0.05$.

3 | RESULTS AND DISCUSSION

3.1 | Fabrication of CFs

ALG is a natural-origin polymer that is widely used for fibre fabrication due to its fast ionic cross-linking in the presence of divalent ions, such as Ca^{2+} or Mg^{2+} (Akbari et al., 2014; Costa-Almeida et al., 2016; Lee & Mooney, 2012; Tamayol et al., 2015). Gelatin is a denatured form of collagen, with interesting advantages over native collagen, including better solubility and reduced antigenicity. GelMA has been successfully used for three-dimensional culture of various cells and engineering different tissues (Yue, Alvarez, Tamayol, Annabi, & Khademhosseini, 2015) and can provide suitable biological cues for cellular growth.

We used commercially available multifilament silk suture threads (Figure 1) that were further coated with a mixture of 1.5% (*w*/*v*) ALG and 10% (*w*/*v*) GelMA (Figure 1) to create a hydrogel layer. Suture threads were coated following a protocol similar to the one previously described by our team (Akbari et al., 2014). It should be noted that the approach is robust and can be applied to bioresorbable sutures. Herein, ALG was used to generate an auxiliary network physically entrapping GelMA until its photocrosslinking by exposure to ultraviolet light. The use of such ALG network has been proven to result in a more robust strategy for hydrogel fibre fabrication, enabling an easier manual handling by improving the mechanical strength of developed fibres (Costa-Almeida et al., 2016; Tamayol et al., 2015). CFs were obtained with a hydrogel thickness of 137 ± 31 μm. Nonetheless, as previously demonstrated, this parameter can be easily tailored by varying prepolymer concentration (viscosity) and coating speed (Akbari et al., 2014).

3.2 | Viability of encapsulated cells

The biological activity of CFs was evaluated by encapsulating hTDCs (Figure 2a and 2b). Upon encapsulation, cell viability and metabolic activity were determined by live/dead (Figure 2c, 2d, and 2f–2h) and Alamar Blue (Figure 2e) assays, respectively. Our results indicated that encapsulated cells remained alive up to at least 21 days. The high cellular

viability on the first day of culture (Figure 2c) indicates that the fabrication process was harmless to the cells. Moreover, cellular metabolic activity increased overtime, as determined by Alamar Blue assay, which indicates that the CFs supported cellular growth (Figure 2e). The reduction in metabolic activity after 14 days is mainly explained by cell migration from the hydrogel outwards, due to the limited surface area of the fibre. Nonetheless, encapsulated hTDCs are viable up to 21 days in culture (Figure 2f–2h), and the hydrogel layer seemed to be stable over time (Figure 2g). In our previously reported CFs, the hydrogel layer was composed of ALG, which resulted in diminished cell viability 7 days after encapsulation (Akbari et al., 2014). Herein, the incorporation of GelMA seemed to be beneficial in maintaining cellular activities overtime. Indeed, although ALG lacks suitable adhesion cues for supporting long-term cell function, GelMA contains cell-binding motifs, like arginine-glycine-aspartic acid sequences, and matrix metalloproteinases (MMP)-sensitive degradation sites required for cell remodelling, enabling cell proliferation and migration within GelMA-based hydrogels, as supported by the results discussed below.

3.3 | Cell alignment and matrix production

Cell distribution and organization, as well as ECM deposition were studied in CFs. Interestingly, encapsulated hTDCs migrated within the hydrogel matrix reaching the core fibre and aligning along the direction of the microfibres composing the suture threads, as observed by the F-actin staining of cytoskeletal filaments after 21 days (Figure 3a and 3b). Indeed, two cell-populated regions could be distinguished within CFs at Day 7, corresponding to cells encapsulated in the hydrogel layer and cells elongated and aligned at the surface of the core thread (Figure S1). This result supports the versatility of our strategy with the hydrogel acting as a protective reservoir for encapsulated cells, which were able to migrate and followed the topographical cues provided by the core thread. Topography plays an essential role in modulating cellular activities through contact guidance, including cell differentiation. Human tendon stem cells cultured on aligned nanofibres have been demonstrated to express significantly higher levels of tendon-related genes and to escape osteogenic induction, in comparison to cells cultured on random nanofibres (Yin *et al.*, 2010). Herein, we observed that hTDCs remodelled their micro-environment, a critical step for prospective in vivo application of a tissue engineered construct. Between 7 and 21 days, hTDCs were able to synthesize a collagen-rich matrix (Figure 3c–3e), which is a main component of natural tendon niche. Particularly, collagen type I was detected intracellularly, being expressed by cells aligned on the fibres (Figure 3c and 3d). Besides, after 21 days in culture, a notable layer of collagen type III covering the surface of the suture thread was observed (Figure 3e), in comparison to earlier periods of culture (Figure S2).

The cellular remodelling within the ALG:GelMA hydrogel layer (Figure 3g) resulted in the formation of a well-aligned matrix after 21 days, as observed by scanning electron microscopy analysis (Figure 3h). Strikingly, the morphology of hTDCs-laden CFs upon this period of culture was comparable to the aligned structure of native tendon tissue (Figure 3i). Moreover, the alignment of CFs cultured for 1 and 21 days was quantified and compared using 2D-FFT analysis. Matrix alignment is evident in CFs after 21 days (Figure 3f and 3h), as seen by the two symmetric sharp peaks suggesting anisotropic alignment, which is less evident at Day 1 (Figure 3f and 3g). Thus, the proposed core-shell composite fibre approach

constitutes a platform that stimulates human tendon cells to start engineering their own tendon-specific micro-environment.

3.4 | Phenotype of encapsulated cells

To further characterize encapsultated hTDCs, gene expression analysis was performed by quantitative RT-PCR to evaluate the expression of tendon-related genes and genes associated to ECM remodelling, as well as to assess phenotypic drift towards osteogenic differentiation (Figure 4).

Scleraxis (*SCX*) and Mohawk (*MKX)* are two transcription factors that exist in developing tendons and are associated to tenogenic differentiation (Ito et al., 2010; Murchison et al., 2007). Herein, the expression of *SCX* (Figure 4a) was significantly up-regulated in encapsulated hTDCs after 7 days in culture (approximately six-fold, $p < 0.01$, in comparison to hTDCs at Day 0), whereas *MKX* transcript levels were similar to those of control cells (hTDCs at Day 0) over time in culture (Figure 4b). Strikingly, *SCX*-expressing cells have been recently described to participate in tendon regenerative mechanisms and neonatal tendon healing (Howell et al., 2017). Moreover, tenascin C (*TNC*) is a non-adhesive glycoprotein present in the ECM of tendon stem cell niche (Bi et al., 2007). In our study, *TNC* was significantly up-regulated in encapsulated hTDCs (Figure 4c) after 7 (22-fold, $p < 0.01$) and 21 days (25-fold, $p < 0.01$). Additionally, decorin (*DCN*) is a proteoglycan found in tendon-related ECM that, together with biglycan, is involved in collagen fibrillogenesis during tendon development (Zhang et al., 2006) and in collagen fibril maintenance during tendon homeostasis (Robinson et al., 2017), but is also implicated in scar formation after tendon injury (Nakamura et al., 2000). No differences were found for *DCN* expression in encapsulated hTDCs (Figure 4d), in comparison to control cells.

Furthermore, the expression of genes associated to ECM remodelling was studied, with particular focus on MMP1 (collagenase) and MMP2 (gelatinase), which degrade fibrillar collagen and collagen fragments, respectively. *MMP1* (Figure 4e) and *MMP2* (Figure 4f) were significantly up-regulated in encapsulated hTDCs after 7 days (approximately 195-fold for *MMP1* and approximately 9-fold for *MMP2*, $p < 0.05$ in comparison to hTDCs at Day 0), suggesting that matrix remodelling is rapidly triggered, facilitating the migration of hTDCs from the hydrogel to the core fibre (Figure 3a and 3b).

Moreover, the expression of genes related to osteogenesis, adipo-genesis, and chondrogenic differentiation was examined. Herein, only runt-related transcription factor 2 (*RUNX2*), a transcriptional regulator involved in the early stage of osteoblast differentiation (Huang, Yang, Shao, & Li, 2013), was detected in the population of hTDCs; whereas other osteogenic genes (osteopontin, *SPP1*), as well as adipogenic (leptin, *LEP*; perixysome proliferator-activated receptor gamma 2, *PPARγ2*) and chondrogenic (SRY-box 9, *SOX9*) markers could not be detected (data not shown). Interestingly, *RUNX2* was significantly down-regulated in encapsulated hTDCs after 7 and 21 days in culture, in comparison to control cells ($p < 0.0001$, Figure 4g), supporting that our system directs tenogenesis and may be avoiding the phenotypic drift towards the osteogenic lineage.

Overall, the expression profile of the studied tendon-related genes and genes associated to ECM remodelling, together with the observed collagen deposition, suggest that encapsulated hTDCs may be directed to promote tendon regeneration. Nevertheless, future studies should be focused on the tenogenic differentiation of other cell sources and on assessing the in vivo therapeutic potential of the proposed system.

3.5 | Development of braided constructs

The fabrication of a suitable tendon substitute or artificial graft requires the emulation of adequate mechanical properties that can withstand, not only the physiological loads, but also the additional mechanical requirements during physiotherapy upon graft implantation. Textile technologies, including weaving, knitting, twisting, and braiding, have been widely explored as appealing tools for engineering artificial tissues and organs (Akbari et al., 2016). Particularly, braided structures exhibit the highest axial strength compared to other textile patterns. However, upon assembly of the developed CFs, the mechanical properties of the engineered constructs depend on both the nature of the core reinforcing material and the characteristics of the assembly process, including the relative amount of axial and braiding fibres, braiding angle, fibre size, and braiding pattern. In order to mimic the morphology and mechanical properties of native tendon, different types of braided structures were formed because it is well known that braided structure demonstrates the highest axial strength compared to other textile patterns, which is essential for the physiological function of tendons.

Four fibres were fixed to a single point and then braided together using the following patterns: 1 × 1 biaxial, 2 × 2 biaxial, and 1 × 1 triaxial (Figure 5a and 5b) and were exposed to uniaxial tensile mechanical test. Their mechanical properties were compared with non-braided parallel fibres (control). Figure 5c shows that the structure assembled according to the 1 × 1 biaxial braiding pattern exhibited the highest modulus of 7970 MPa, followed by the 1 × 1 triaxial (7670 MPa). However, no significant differences were observed for tensile strain (Figure 5d and 5f) and maximum load (Figure 5e) in comparison with control. In addition, there are no significant differences between mechanical properties of uncoated and coated fibres (Figure S3), as the core thread tolerates the majority of load.

Engineering mechanically reinforced hydrogel scaffolds has been the subject of a number of studies. For instance, Wang et al. developed core-shell column and sheet scaffolds for skeletal muscle applications using a system in which nanofibres were aligned within a microsheet pattern and a hydrogel was photopolymerized around the fibres (Wang et al., 2015). Similarly, aligned nanofibres have been assembled into a woven fabric, which was then covered with a cell-hydrogel photocrosslinkable solution aiming at developing heart valve tissue engineered solutions (Wu et al., 2016). Such strategies, although mimicking tissue- and cell-level properties, present a limitation regarding the control over cell positioning within scaffolds. In contrast, the assembly of CFs allows for a different cell arrangement by entangling different cell-laden fibres, which results in a precise positioning of cells from the inside outwards of a three-dimensional construct. In a prospective in vivo implantation scenario, such a CFs-based construct would enable tissue regeneration to occur within the dimensions of the whole scaffold, even inside the construct, through an initial

phase of remodelling within the hydrogel layer, while having the mechanical support of the core thread, which is a critical aspect for tendon regeneration.

In order to evaluate the biological performance of three-dimensional braided constructs, we assembled CFs by braiding four cell-laden fibres together using the 1 × 1 biaxial pattern and keeping a wet environment during the process. Given that textile methods impose a considerable mechanical stress to the assembled fibres, we evaluated the stability of the hydrogel layer coated on the suture thread. For this purpose, we first braided composite fibres loaded with fluorescent beads of different colors. Figure 6a shows the integrity of the hydrogel layers immediately after the braiding process. Furthermore, CFs with encapsulated hTDCs were also assembled (Figure 6b) in the presence of culture medium. A 10-cm long CF construct was assembled, and cell viability was determined by live/dead assay after 1 day of culture (Figure 6c and 6d). The number of viable (green) cells indicates that the hydrogel layer may be acting as a protective shell, maintaining the integrity of the cells even during the braiding process, shielding encapsulated cells from the mechanical/shear stress imposed. In addition, encapsulated hTDCs remained viable up to 21 days within the three-dimensional braided constructs (Figures 6e and S4).

Therefore, main advantages of using CFs include the possibility of independently tailoring the properties of two different compartments. Core threads can be fabricated with a desired topography and mechanical properties and can be further assembled by textile techniques. At the same time, the hydrogel layer can be produced with a defined chemical composition and will act as a protective and hydrated micro-environment supporting cellular activities during in vitro tissue construct maturation until implantation. Interestingly, the use of single CFs to bridge injured tendons can similarly benefit from in vitro culture to enable encapsulated cells to engineer their native environment for a more robust application at the injury site. Future studies will be focused on the in vivo implantation of developed constructs in order to unveil their potential for promoting tissue regeneration in tendon defect models.

4 | CONCLUSION

Through the use of braided CFs, three-dimensional cell-laden constructs with clinically relevant dimensions can be fabricated. In particular, the biological performance was investigated at the single fibre level using encapsulated tendon cells. hTDCs were able to migrate within the hydrogel layer, align at the surface of the core thread, and deposit a newly synthesized collagen-rich matrix, generating a tendon-specific micro-environment, even comparable to the organization of native tendon tissue. Thus, CFs supported key aspects for successfully engineering artificial living tendons.

Supplementary Material

Refer to Web version on PubMed Central for supplementary material.

ACKNOWLEDGEMENTS

The authors would like to thank to Hospital da Prelada (Porto, Portugal) for providing human tendon tissue samples; to Portuguese funds through FCT—Fundação para a Ciência e a Tecnologia in the framework of FCT-POPH-FSE, the grants SFRH/BD/96593/2013, SFRH/BPD/112459/2015, and IF/00593/2015 of R. C-A., R. M. A. D., and M. E. G., respectively.

Funding information

Fundação para a Ciência e aTecnologia, Grant/Award Numbers: SFRH/BD/96593/2013, SFRH/BPD/112459/2015 and IF/00593/2015

REFERENCES

Akbari M, Tamayol A, Bagherifard S, Serex L, Mostafalu P, Faramarzi N, … Khademhosseini A (2016). Textile technologies and tissue engineering: A path toward organ weaving. Advanced Healthcare Materials, 5, 751–766. [PubMed: 26924450]

Akbari M, Tamayol A, Laforte V, Annabi N, Najafabadi AH, Khademhosseini A, & Juncker D (2014). Composite living fibers for creating tissue constructs using textile techniques. Advanced Functional Materials, 24, 4060–4067. [PubMed: 25411576]

Ayres CE, Jha BS, Meredith H, Bowman JR, Bowlin GL, Henderson SC, & Simpson DG (2008). Measuring fiber alignment in electrospun scaffolds: A user's guide to the 2D fast Fourier transform approach. Journal of Biomaterials Science. Polymer Edition, 19, 603–621. [PubMed: 18419940]

Bi Y, Ehirchiou D, Kilts TM, Inkson CA, Embree MC, Sonoyama W, ... Young MF (2007). Identification of tendon stem/progenitor cells and the role of the extracellular matrix in their niche. Nature Medicine, 13, 1219–1227.

Costa-Almeida R, Gasperini L, Borges J, Babo PS, Rodrigues MT, Mano JF, … Gomes ME (2016). Multicomponent hydrogel fibers for tendon tissue engineering: Combining polyelectrolyte complexation and microfluidics. ACS Biomaterials Science & Engineering, 3, 1322–1331.

Domingues RMA, Chiera S, Gershovich P, Motta A, Reis RL, & Gomes ME (2016). Enhancing the biomechanical performance of anisotropic nanofibrous scaffolds in tendon tissue engineering: Reinforcement with cellulose nanocrystals. Advanced Healthcare Materials. 5, 1364–1375. [PubMed: 27059281]

Fallahi A, Khademhosseini A, & Tamayol A (2016). Textile processes for engineering tissues with biomimetic architectures and properties. Trends in Biotechnology, 34, 683–685. [PubMed: 27499277]

Howell K, Chien C, Bell R, Laudier D, Tufa SF, Keene DR, … Huang AH (2017). Novel model of tendon regeneration reveals distinct cell mechanisms underlying regenerative and fibrotic tendon healing. Scientific Reports, 7, 45238. [PubMed: 28332620]

Huang W, Yang S, Shao J, & Li Y-P (2013). Signaling and transcriptional regulation in osteoblast commitment and differentiation. Frontiers in Bioscience, 12, 3068–3092.

Ito Y, Toriuchi N, Yoshitaka T, Ueno-Kudoh H, Sato T, Yokoyama S, … Asahara H (2010). The Mohawk homeobox gene is a critical regulator of tendon differentiation. Proceedings of the National Academy of Sciences of the United States of America, 107, 10538–10542. [PubMed: 20498044]

Kang E, Jeong GS, Choi YY, Lee KH, Khademhosseini A, & Lee S-H (2011). Digitally tunable physicochemical coding of material composition and topography in continuous microfibres. Nature Materials, 10, 877–883. [PubMed: 21892177]

Lee KY, & Mooney DJ (2012). Alginate: Properties and biomedical applications. Progress in Polymer Science, 37, 106–126. [PubMed: 22125349]

Livak KJ, & Schmittgen TD (2001). Analysis of relative gene expression data using real-time quantitative PCR and the 2-ΔΔCT method. Methods, 25, 402–408. [PubMed: 11846609]

Lomas AJ, Ryan CNM, Sorushanova A, Shologu N, Sideri AI, Tsioli V, … Zeugolis DI (2015). The past, present and future in scaffold-based tendon treatments. Advanced Drug Delivery Reviews, 84, 257–277. [PubMed: 25499820]

Murchison ND, Price BA, Conner DA, Keene DR, Olson EN, Tabin CJ, & Schweitzer R (2007). Regulation of tendon differentiation by scleraxis distinguishes force-transmitting tendons from muscle-anchoring tendons. Development, 134, 2697–2708. [PubMed: 17567668]

Nakamura N, Hart DA, Boorman RS, Kaneda Y, Shrive NG, Marchuk LL, … Frank CB (2000). Decorin antisense gene therapy improves functional healing of early rabbit ligament scar with enhanced collagen fibrillogenesis in vivo. Journal of Orthopaedic Research, 18, 517–523. [PubMed: 11052486]

Onoe H, Okitsu T, Itou A, Kato-Negishi M, Gojo R, Kiriya D, … Takeuchi S (2013). Metre-long cell-laden microfibres exhibit tissue morphologies and functions. Nature Materials, 584–590. [PubMed: 23542870]

Robinson KA, Sun M, Barnum CE, Weiss SN, Huegel J, Shetye SS, … Birk DE (2017). Decorin and biglycan are necessary for maintaining collagen fibril structure, fiber realignment, and mechanical properties of mature tendons. Matrix Biology. 10.1016/j.matbio.2017.08.004.

Schmittgen TD, & Livak KJ (2008). Analyzing real-time PCR data by the comparative CT method. Nature Protocols, 3, 1101–1108. [PubMed: 18546601]

Sibaja B, Culbertson E, Marshall P, Boy R, Broughton RM, Solano AA, … Auad ML (2015). Preparation of alginate–chitosan fibers with potential biomedical applications. Carbohydrate Polymers, 134, 598–608. [PubMed: 26428163]

Tamayol A, Najafabadi AH, Aliakbarian B, Arab-Tehrany E, Akbari M, Annabi N, … Khademhosseini A (2015). Hydrogel templates for rapid manufacturing of bioactive fibers and 3D constructs. Advanced Healthcare Materials, 4, 2146–2153. [PubMed: 26304467]

Wang L, Wu Y, Guo B, & Ma PX (2015). Nanofiber yarn/hydrogel core shell scaffolds mimicking native skeletal muscle tissue for guiding 3D myoblast alignment, elongation, and differentiation. ACS Nano, 9, 9167–9179. [PubMed: 26280983]

Wu S, Duan B, Liu P, Zhang C, Qin X, & Butcher JT (2016). Fabrication of aligned nanofiber polymer yarn networks for anisotropic soft tissue scaffolds. ACS Applied Materials & Interfaces, 8, 16950–16960. [PubMed: 27304080]

Yin Z, Chen X, Chen JL, Shen WL, Nguyen TMH, Gao L, & Ouyang HW (2010). The regulation of tendon stem cell differentiation by the alignment of nanofibers. Biomaterials, 31, 2163–2175. [PubMed: 19995669]

Younesi M, Islam A, Kishore V, Anderson JM, & Akkus O (2014). Tenogenic induction of human MSCs by anisotropically aligned collagen biotextiles. Advanced Functional Materials, 24, 5762–5770. [PubMed: 25750610]

Yue K, GT-d S, Alvarez MM, Tamayol A, Annabi N, & Khademhosseini A (2015). Synthesis, properties, and biomedical applications of gelatin methacryloyl (GelMA) hydrogels. Biomaterials, 73, 254–271. [PubMed: 26414409]

Zhang G, Ezura Y, Chervoneva I, Robinson PS, Beason DP, Carine ET, … Birk DE (2006). Decorin regulates assembly of collagen fibrils and acquisition of biomechanical properties during tendon development. Journal of Cellular Biochemistry, 98, 1436–1449. [PubMed: 16518859]

Zhang J, Wang L, Zhu M, Wang L, Xiao N, & Kong D (2014). Wet-spun poly(ε-caprolactone) microfiber scaffolds for oriented growth and infiltration of smooth muscle cells. Materials Letters, 132, 59–62.

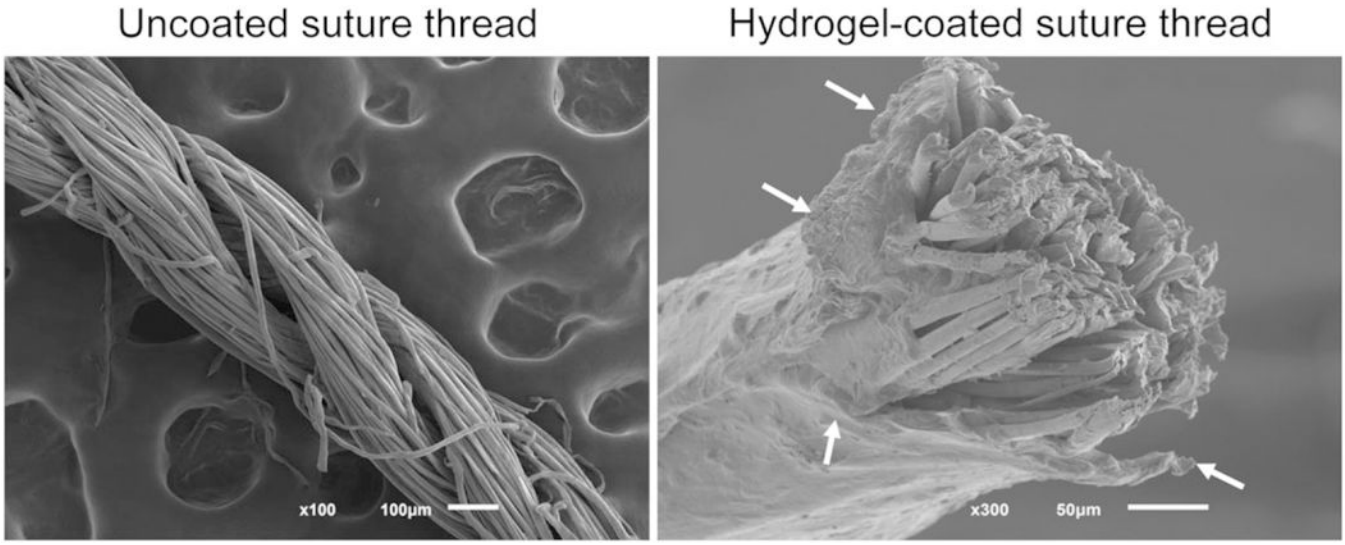

FIGURE 1.

Scanning electron microscope images of uncoated and hydrogel-coated suture threads. Arrows indicate the hydrogel layer covering the core fibre

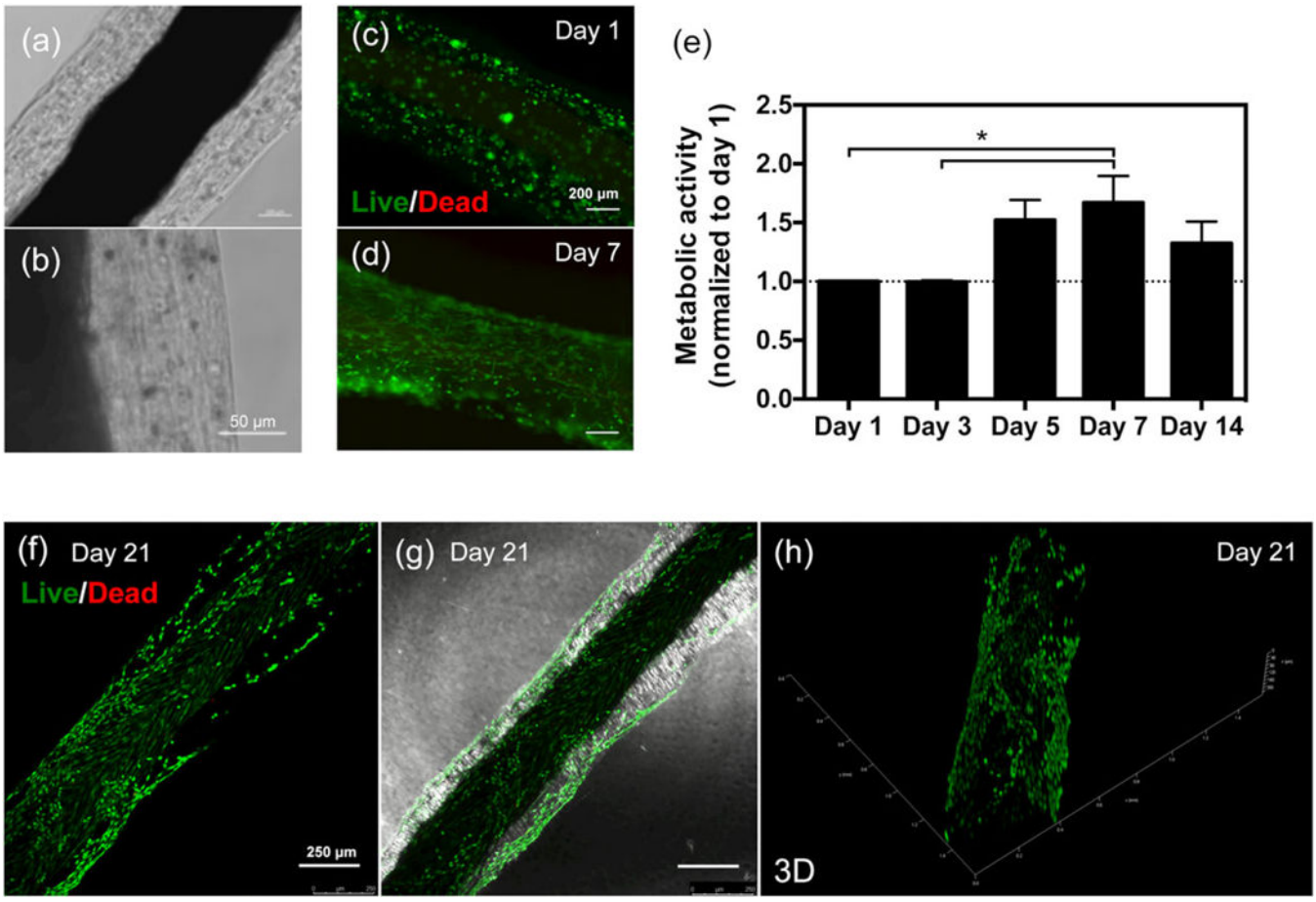

FIGURE 2.

Viability of human tendon-derived cells encapsulated in composite fibres. (a and b) Optical microscope images of cell-laden composite fibres after 7 days in culture. Scale bars, (a) 100 and (b) 50 μm. (c and d) Live/dead images of human tendon-derived cells encapsulated within composite fibres after (c) 1 and (d) 7 days in culture. Live cells are green (calcein acetoxymethyl), and dead cells are red (propidium iodide). (e) Cellular metabolic activity determined using Alamar Blue assay. Results are normalized with respect to the values for Day 1. Statistically significant differences are shown as $*p < 0.05$. (f–h) Confocal microscope images of live/dead staining of human tendon-derived cells encapsulated within composite fibres after 21 days in culture. (g) Live/dead image merged with brightfield channel. Scale bars, 250 μm. (h) Three-dimensional reconstruction [Colour figure can be viewed at wileyonlinelibrary.com]

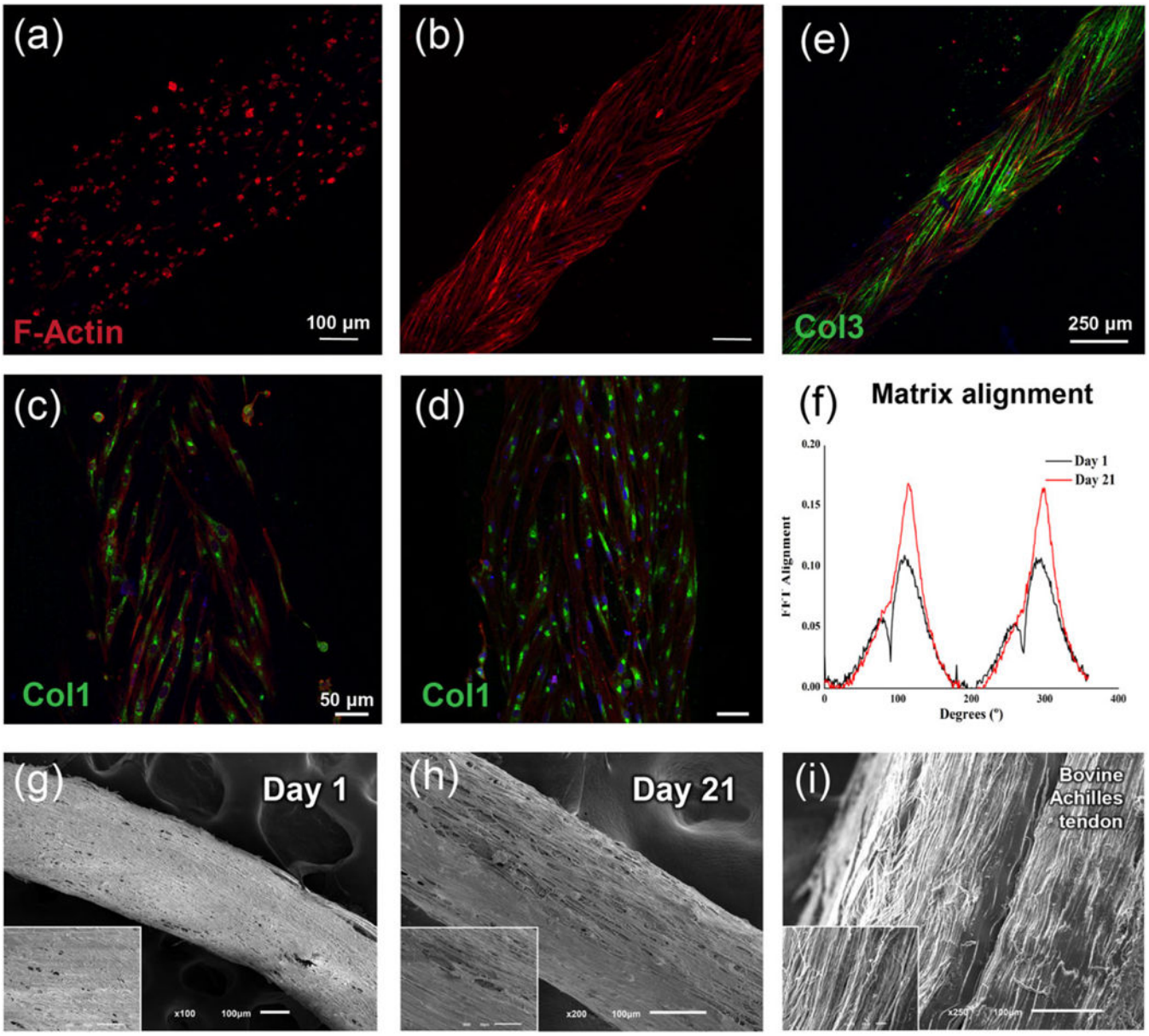

FIGURE 3.

Behavior of human tendon-derived cells encapsulated in composite fibres. (a and b) F-actin staining of encapsulated human tendon-derived cells showing cell migration from the hydrogel layer (Day 3, a) to the surface of the core fibre (Day 21, b). (c and d) Collagen type I immunostaining (green) of encapsulated human tendon-derived cells after (c) 7 and (d) 14 days in culture. Scale bars, 50 μm. (e) Immunostaining against collagen type III (green) after 21 days in culture. Scale bar, 250 μm. Cell cytoskeleton and cell nuclei were counterstained with F-actin (red) and 4',6-diamidino-2-phenylindole (blue), respectively. (f) Two-dimensional fast Fourier transform frequency plots comparing matrix alignment between Day 1 and Day 21 of culture. (g–i) Scanning electron microscope images of composite fibres after (g) 1 and (h) 21 days in culture, scale bar, 100 um; (inset) higher magnifications, scale bar, 50 μm. (i) Scanning electron microscope images of bovine Achilles tendon, scale bar,

100 μm; (inset) higher magnifications, scale bar, 100 μm [Colour figure can be viewed at wileyonlinelibrary.com]

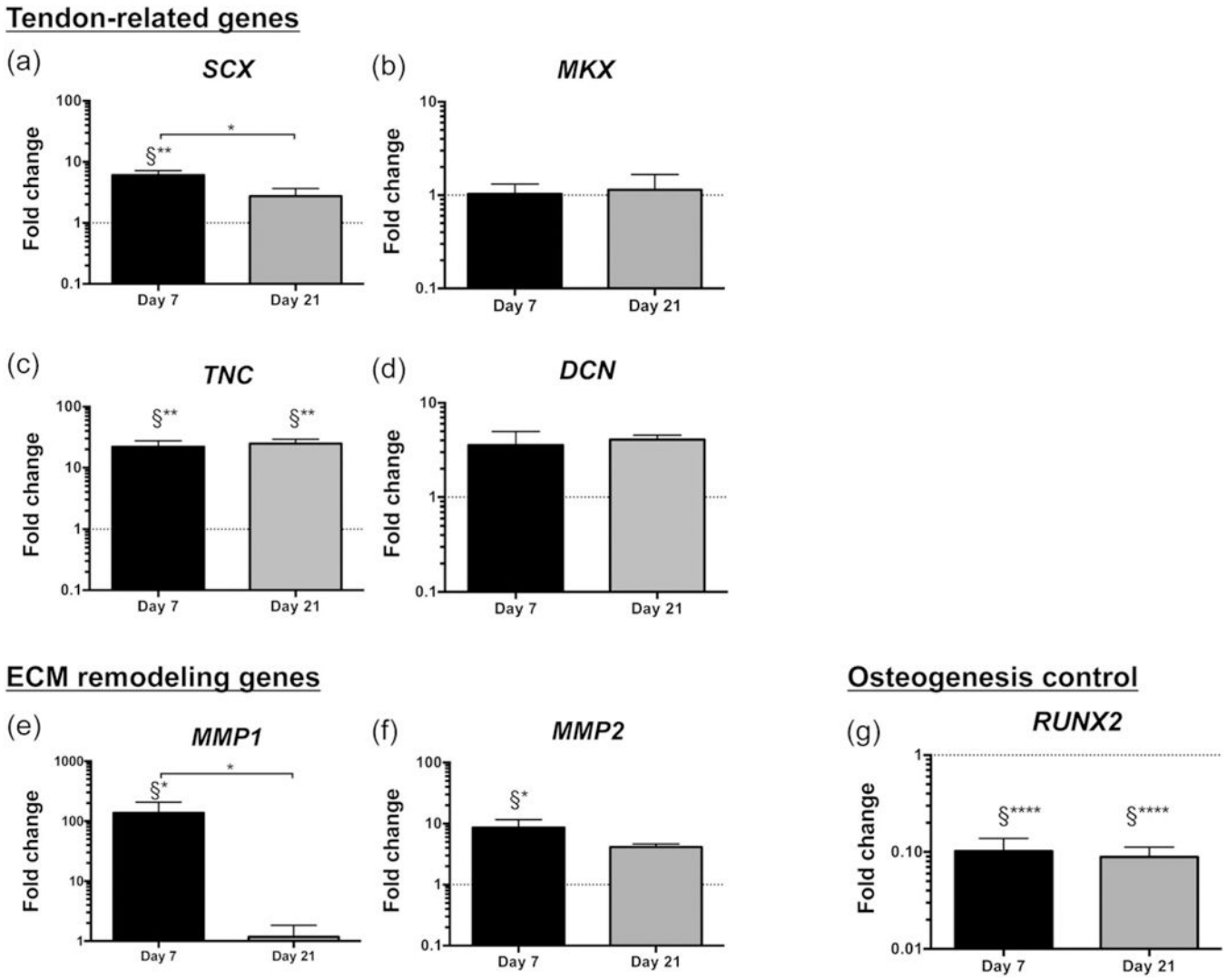

FIGURE 4.

Phenotypic characterization of encapsulated human tendon-derived cells after 7 and 21 days in culture. (a–d) Expression of tendon-related genes: (a) *SCX*, scleraxis; (b) *MKX*, Mohawk; (c) *TNC*, tenascin C; (d) *DCN*, decorin. (e–f) Expression of genes associated to extracellular matrix (ECM) remodelling: (e) *MMP1*, matrix metalloproteinase 1; (f) *MMP2*, matrix metalloproteinase 2. (g) Expression of osteogenesis-related gene, *RUNX2*, runt-related transcription factor 2. Expression of target genes was normalized to glyceraldehyde 3-phosphate dehydrogenase housekeeping gene. Gene expression at different time points was normalized to day 0 of human tendon-derived cells (calibrator sample). Results are presented as mean ± standard error of the mean ($n = 12$). Statistically significant differences are shown as *$p < 0.05$; **$p < 0.01$; ****$p < 0.0001$; §Statistically significant differences in comparison to calibrator sample (human tendon-derived cells, Day 0)

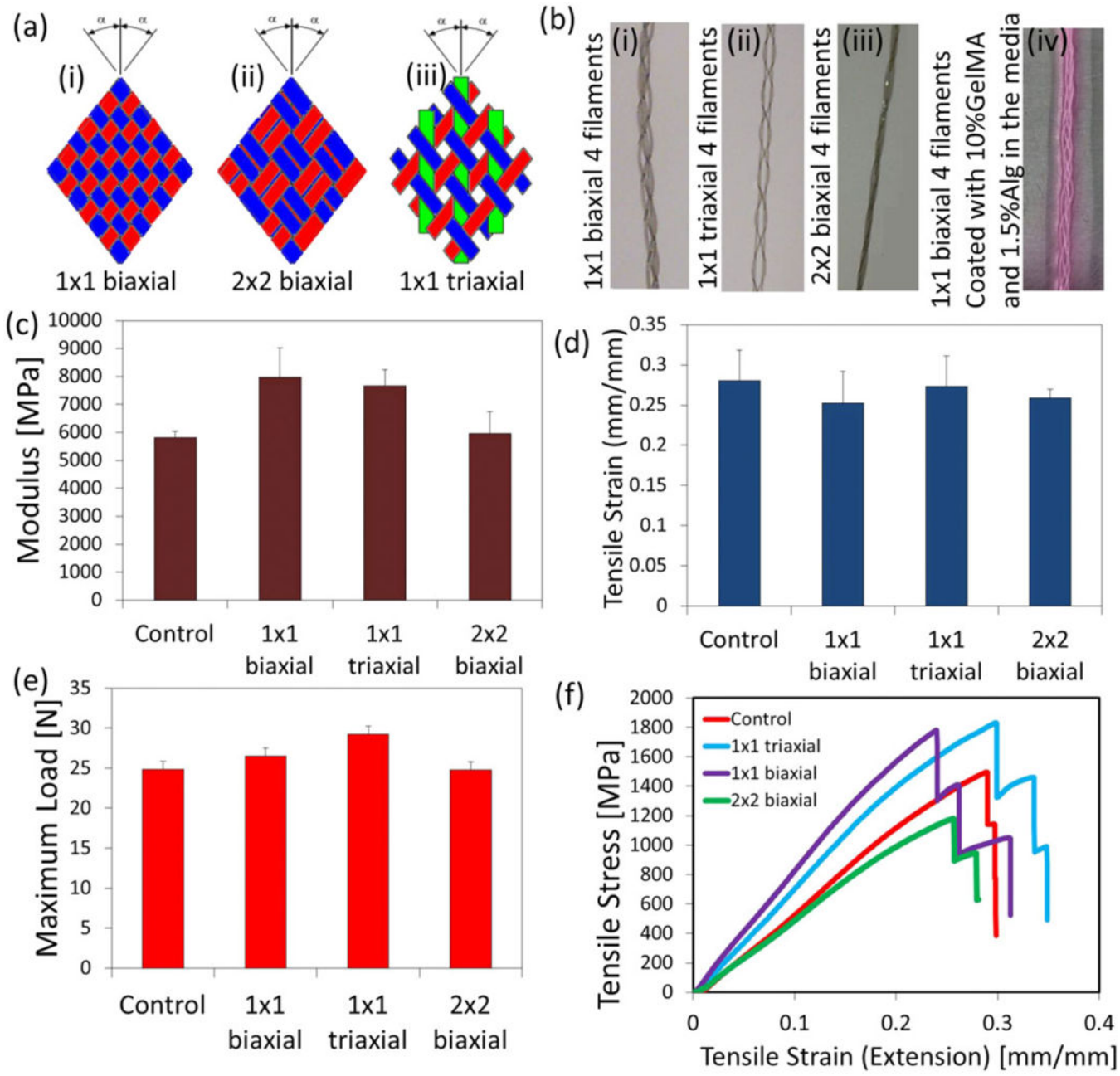

FIGURE 5.

Mechanical properties of braided suture threads: (a) Schematic of three different braiding systems: (i) 1 × 1 biaxial; (ii) 2 × 2 biaxial; (iii) 1 × 1 triaxial; (b) four braided suture filaments with different methods mentioned in (a) and (iv) 1 × 1 biaxial coated with 10% methacrylated gelatin and 1.5% alginate in the media; (c) modulus (MPa); (d) tensile strain (mm/mm); (e) maximum load (*N*); (f) tensile stress versus tensile strain for different braiding styles [Colour figure can be viewed at wileyonlinelibrary.com]

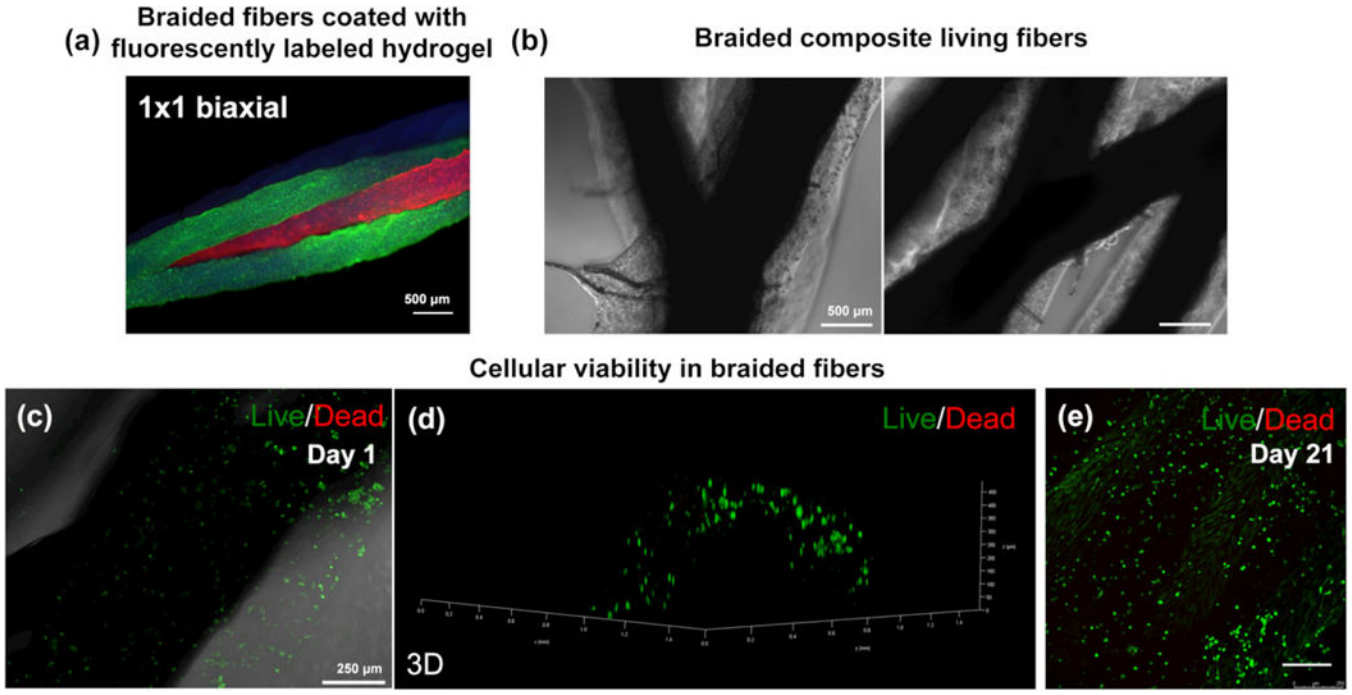

FIGURE 6.

Assembly of composite fibres and cellular viability. (a) Fluorescent microbead-laden ALG:GelMA fibres assembled in a three-dimensional construct using 1 × 1 biaxial braiding pattern. (b) Braided composite fibres showing the intersection of the pattern and the four fibre strands in the construct. (c) Live/dead image of human tendon-derived cells encapsulated within composite fibres 1 day after braiding and (d) respective three-dimensional reconstruction. (e) Live/dead image of human tendon-derived cells encapsulated within braided constructs after 21 days of culture [Colour figure can be viewed at wileyonlinelibrary.com]